*clean technologies*

MDPI

*Article*

# Application of Carboxymethyl Cellulose (CMC)-Coated Nanoscale Zero-Valent Iron in Chromium-Containing Soil Remediation

**Bo Zhang [1], Jiani Zhan [1,*], Jiaqi Fan [1,*], Bohong Zhu [1], Weili Shen [1], Shiwei Zhang [1], Weiting Li [1], Zhaohui Li [2] and Fanjun Zeng [2]**

[1] College of Materials and Advanced Manufacturing, Hunan University of Technology, Zhuzhou 421000, China; 13747@hut.edu.cn (B.Z.); bohongzhu@hut.edu.cn (B.Z.); 13107021269@163.com (W.S.); 13833849135@163.com (S.Z.); 17670353640@139.com (W.L.)

[2] Linwu Xiangxin Kaishun Water Service Co., Chenzhou 424300, China; wangyq20229@126.com (Z.L.); 13031053966@163.com (F.Z.)

* Correspondence: ariesalyssa@outlook.com (J.Z.); jiaqifan942674@foxmail.com (J.F.); Tel.: +86-155-7378-1779 (J.Z.); +86-152-4378-3039 (J.F.)

**Abstract:** Nanofine zero−valent iron (nZVI) is a new, eco−friendly material with strong reducing and adsorbent properties that can be used to clean up heavy metal−affected soils. Herein, nZVI encapsulated with carboxymethyl cellulose (CMC−nZVI) is synthesized via an aqueous−phase reduction technique and subsequently deployed to evaluate its effectiveness in Cr(VI) soil remediation. The characterization analysis used SEM−EDS, XRD, XPS, and LSV to determine the relevant properties of the material. The results show that at an initial Cr(VI) concentration of 169.5 mg·kg$^{-1}$, 93.2% of Cr(VI) was removed from the soil after 10 h of treatment with CMC−nZVI at pH 3.3. The kinetic analysis showed that CMC−nZVI had the maximum equilibrium adsorption capacity for removing Cr(VI) from soil at 105.3 mg·g$^{-1}$. This followed a pseudo−second−order kinetic model. The study shows that CMC−nZVI converts Cr(VI) to Cr(III), which forms complexes with Fe(III) ions in the presence of hydroxide ions ($OH^-$) to form a highly stable compound that eventually adsorbs into the nanomaterial's surface for efficient removal.

**Keywords:** CMC−coated nanoscale zero−valent iron; removal; chromium−containing soil; removal mechanism



**Citation:** Zhang, B.; Zhan, J.; Fan, J.; Zhu, B.; Shen, W.; Zhang, S.; Li, W.; Li, Z.; Zeng, F. Application of Carboxymethyl Cellulose (CMC)-Coated Nanoscale Zero-Valent Iron in Chromium-Containing Soil Remediation. *Clean Technol.* **2024**, *6*, 1610–1624. https://doi.org/10.3390/cleantechnol6040078

Academic Editor: Mentore Vaccari

Received: 13 September 2024
Revised: 10 November 2024
Accepted: 25 November 2024
Published: 11 December 2024



## 1. Introduction

Rapid economic development is often accompanied by industrial damage to the environment, which results in severe contamination of soil resources, such as heavy metal pollution. In particular, high chromium concentrations are found in factories in the electroplating, textile, and metallurgical industries [1]. Moreover, trivalent chromium and hexavalent chromium are commonly used in industry, making chromium in contaminated soil present in these two valence forms [2]. Many nations and areas consider Cr(VI) to be one of the priority pollutants [3,4]. Under natural conditions, Cr(VI) exists in a stable and crystalline form with high stability. In polluted soils, the leachability of Cr(VI) is greatly increased, facilitating its entry into the ecosystem and accumulation in plants, notably crops, via soil migration, thereby endangering human and animal health [5]. It would seem, then, that the pollution management of Cr(VI), a heavy metal in the soil, has become an urgent environmental problem.

Recently, a new nanomaterial restoration technology has been attracting increasing attention because of its good eco−friendly properties and high efficiency [6]. It is thought that the freshly made nZVI has a high diffusivity 'r' in soil because of its improved mobility, a large specific surface area, and high reactivity [7]. According to certain research, nZVI is frequently utilized in a variety of environmental treatments, including dye [8], phenol [9], and some heavy metals [10,11]. However, the magnetic and van der Waals forces present in

bare nZVI severely affect the dispersion of the material [12], causing particles to aggregate and form micron−sized flocs. This ultimately reduces the mobility of nZVI particles and the efficiency of remediation of pollutants. It has been suggested that a variety of materials could be used to modify nZVI in order to prevent aggregation and improve the persistence of its dispersion. These include biochar [13], chelating agents [14], bentonite [15], clay [16], and anionic polymers [17]. In particular, food−grade sodium anionic polymers, such as CMC, have been widely used to stabilize nZVI particles [18,19]. In addition, it was found that nZVI stabilized with CMC is also a very effective Cr(VI) reducing agent [20].

Although modified nZVI has been used extensively for removing heavy metal ions from contaminated waters, few researchers have focused on the remediation of chromium −containing soils by CMC−nZVI. Soil experiments are more complex and have more influencing factors compared with water treatment experiments. The detection of the experimental results is also more complicated than for water treatment, with soil tests adding drying and leaching steps and taking a longer time. For this reason, a CMC−nZVI treatment method for Cr(VI)−contaminated soil is needed, along with a study of the impact of other parameters on the remediation ability (such as the type of material, the amount of material, the starting pH of the soil, and the beginning Cr(VI) concentration of the soil). Examining how CMC−coated nZVI aids in soil detoxification from hexavalent chromium is crucial.

This research successfully produced nZVI stabilized with carboxymethyl cellulose (CMC−nZVI) and assessed its efficacy in addressing soil contamination by chromium in its hexavalent form. Furthermore, an attempt was made to quantify the characteristics of CMC−nZVI and assess its removal efficiency for hexavalent chromium. Furthermore, the potential mechanisms of Cr(VI) adsorption, reduction, and precipitation complexation in soil by CMC−nZVI were also explored, which provided valuable insights and technical guidance for the on−site treatment of heavy−metal−contaminated soil areas with CMC−nZVI.

## 2. Materials and Methods

### *2.1. Materials*

Experimental chemicals are shown in Table S1 of the Supplementary Material. The following reagents were all of analytical purity grade and approved for direct use without further processing. The entire experiment was conducted with deionized water.

### *2.2. Analysis and Sampling of Soil*

This study utilized soil samples collected from four different areas of the former Changsha Chromite Factory (latitude 28°11′49″ N and longitude 112°58′42″ E). Four groups of soil were air−dried and ground into small particles; subsequently, these materials were sifted using a sieve with a mesh size of 1 mm to prepare them for the following experimental procedures. The characteristics of the soil were examined according to standard protocols [21,22]. The soil texture was comprised of clay and sand, with respective proportions of 99.2% and 0.8%. Using the DTPA extraction method (GB/T 23739–2009) [23], the Cr(VI) values in four distinct locations were 101.2, 169.5, 202.2, and 315.2 $mg \cdot kg^{-1}$, in that order. Meanwhile, the pH was approximately 6.8 based on the diphenylcarbodihydrazide spectrophotometry method (GB 7467–87) [24].

### *2.3. CMC−nZVI Synthesis*

The CMC−nZVI was synthesized with CMC as a coating material, while the nZVI was generated by liquid−phase reduction. Different CMC−nZVI were synthesized by varying mass ratios of CMC and iron ($M_{CMC}$:$M_{iron}$ = 0.5:1, 1:1, or 2:1) as follows. To summarize, within a 500 mL flask featuring three necks, a mixture comprising 100 mL of ethanol and purified water (80% volume fraction, purged with pure argon gas for 60 min to eliminate dissolved oxygen) was prepared, and 1.21 g of $FeCl_3 \cdot 6H_2O$ was dissolved under mechanical stirring and a continuous flow of pure argon. Subsequently, we explored the possibility

of reducing the aggregation of nZVI particles by introducing a newly formulated $NaBH_4$ solution (0.34 g $NaBH_4$ added to 50 mL solution) into the above solution. Finally, under the condition of mechanical agitation, different quantities of CMC (0.125, 0.25, or 0.50 g, each in a 10 mL volume) were introduced into the solution and stirred for 20 min, thereby obtaining CMC−nZVI, which contains 0.25 g of nZVI. Equation (1) provides a helpful representation of the reaction.

$$4Fe^{3+} + 3BH_4^- + 9H_2O \rightarrow 4Fe^0{}_{(s)} \downarrow + 3H_2BO_3^-{}_{(aq)} + 12H^+ + 6H_{2(g)} \uparrow \quad (1)$$

After the aforementioned procedure, vacuum filtration was used to remove the black particles, and anhydrous ethanol was used to rinse them. Furthermore, the resulting material was vacuum−dried at 60 °C for 48 h.

### *2.4. Materials Characterization*

#### 2.4.1. Characterization of nZVI Before and After Coating

Freshly prepared nZVI and CMC−nZVI were freeze−dried and ground into fine particles in an anaerobic environment for characterization experiments. The shape and dimensions of the materials, both pre− and post−coating, were examined using a JSM−7500F Scanning Electron Microscope (SEM) from Applied Scientific Instruments (Shanghai) Co., Ltd. (Shanghai, China). Concurrently, the BET surface area was measured using a PM7240 Brunauer–Emmett–Teller (BET) analyzer from Huapu Hengchuang Instruments (Beijing) Co., Ltd. (Beijing, China). Additionally, the material composition was characterized using a D8−ADVANCE X−ray diffractometer (XRD) from Softron Biotechnology (Beijing) Co., Ltd. (Beijing, China) and a Thermo Kalpha X−ray photoelectron spectrometer (XPS) from Thermo Fisher Scientific, Waltham, MA, USA. Anodic polarization curves of both nZVI and CMC−nZVI were examined by electrochemical workstations (LSV, CHI760E, Hangzhou Junsheng Scientific Equipment Co., Ltd. (Hangzhou, China)).

#### 2.4.2. Cr(VI) Characteristics Both Before and After CMC−nZVI Treatment

SEM was used to examine the CMC−nZVI's morphology both before and after the soil treatment. The sample's elemental makeup and distribution within a specific zone were identified using an Energy Dispersive Spectroscope (EDS, Hitachi Regulus 8100, FEI, Hillsboro, Oregon, USA) system, which is part of the Scanning Electron Microscopy setup. The materials were analyzed for elemental composition and chemical morphology using XRD and XPS.

#### 2.4.3. Recovery of CMC−nZVI

A 500 mL beaker containing the CMC−nZVI−treated soil was filled with 200 mL of anhydrous ethanol, which was constantly agitated to ensure complete mixing. The uniformly mixed soil was slowly poured into the magnetic separator (XCGS−50, Jiangxi Barrick Mineral Processing Equipment Co., Ltd., Jiangxi, China) to recover CMC−nZVI. Finally, the collected CMC−nZVI was dried by a freeze−drying machine.

### *2.5. Batch Experiments*

#### 2.5.1. Coating Ratio Investigation Experiment

Variants of CMC−nZVI, each with distinct coating ratios, were synthesized employing the liquid−phase reduction method. They were labeled as control samples, sample No. 1, sample No. 2, and sample No. 3 ($M_{CMC}$:$M_{iron}$ = 0:1, 0.5:1, 1:1, and 2:1, respectively). The four materials were placed in different vessels, and six time periods of 0 h, 1 h, 1 d, 3 d, 5 d, and 7 d were photographed to observe the oxidation of each group.

After adding 200 mL of potassium dichromate solution to a 500 mL flask and mechanically stirring the liquid at room temperature at 300 rpm, the experiment for the removal of Cr(VI) was carried out. The addition of CMC−nZVI initiated the reaction. At intervals (5, 10, 20, 30, 40, 50, 60, and 90 min), 10 mL of solution was collected and centrifugally

filtered for subsequent analysis. The primary reaction parameters utilized in the experiment were CMC−nZVI to treat a chromium(VI) solution with a concentration of 128 mg·L$^{-1}$ at 20 °C and a pH of 7. The mass ratios (support ratios) of CMC to nZVI solid were 0:1 (bare nZVI), 0.5:1, 1:1, and 2:1, with an application rate of 1.25 g·L$^{-1}$. A UV–Vis spectrophotometer (UV−4800, UNICO (Shanghai) Instrument Co., Ltd. (Shanghai, China)) was used to measure Cr(VI) content in the solution. The average values of the three experimental outcomes were the final results, and three duplicates of each experiment were conducted.

#### 2.5.2. Experiments for Cr(VI) Removal in Soils

A 1000 mL beaker was filled with 500 g of precisely weighed soil. Then, the specified doses of nZVI solids were diluted with deionized water so that the particles were uniformly dispersed in the solution. To ensure that the water content of each soil was the same, dry soil was used for this experiment. The amount of deionized water used was 30% of the soil mass. Lastly, a mixer was used to completely mix the previously described solution into the soil. Up to this point, the experimental reaction was activated. First, 20 g of soil was quantitatively sampled at regular intervals (0.5, 2, 4, 6, 8, and 10 h). After drying the soil at high temperatures to stop the nZVI and Cr reactions from continuing, the leaching method was used to assess the Cr concentration (GB/T 23739–2009 and GB 7467–87). Taking into account three different factors, the study assessed how well CMC−nZVI removed Cr(VI) from the polluted soil. The study assessed different factors: initial Cr(VI) concentrations in soil (101.2, 169.5, 202.2, and 315.2 mg·kg$^{-1}$), initial soil pH levels (3.3, 5.1, 6.8, 8.7, and 10.1), and CMC−nZVI quantities applied (0.5, 1.0, 1.5, and 3.0 g·kg$^{-1}$).

### *2.6. Data Analysis and Processing*

The treated Cr(VI) solution was slowly poured into a cuvette measuring 25 mm. With a UV–Vis spectrophotometer, we measured the absorbance at 540 nm to find the amount of Cr(VI) in the solution [25]. The removal rate (R) and adsorption capacity (q) of Cr(VI) were calculated using Equations (2) and (3). In order to gain a deeper understanding of the characteristics of the adsorption process, the experimental data of CMC−nZVI for the removal of Cr(VI) at different pH levels were fitted by the pseudo−first−order kinetic equation (see Equation (4)) and the pseudo−second−order kinetic equation (see Equation (5)). The experimental data of CMC−nZVI for the removal of Cr(VI) at various pH levels were fitted using the pseudo−first−order kinetic equation (see Equation (4)) and the pseudo−second−order kinetic equation (see Equation (5)) in order to examine the characteristics of the adsorption process. The kinetic model categorized as pseudo−first−order indicated a physical adsorption phenomenon; conversely, a chemical adsorption mechanism was suggested by the pseudo−second−order kinetic model.

$$R = \frac{C_0 - C_t}{C_0} \times 100\% \quad (2)$$

$$q = \frac{m}{M} \quad (3)$$

$$\ln(q_e - q_t) = \ln q_e - k_1 t \quad (4)$$

$$\frac{t}{q_t} = \frac{1}{k_2 q_e^2} + \frac{t}{q_e} \quad (5)$$

where $R$—removal rate (%), $C_0$—initial mass concentration (mg·L$^{-1}$ or mg·kg$^{-1}$), $C_t$—the mass concentration at time $t$ during the reaction (mg·L$^{-1}$ or mg·kg$^{-1}$), $q$—removal capacity (mg·g$^{-1}$), $M$—the dosage of CMC−nZVI (g), $m$—removal of Cr (mg), $q_e$—equilibrium adsorption (mg·g$^{-1}$), $q_t$—adsorption at time t (mg·g$^{-1}$), $k_1$—pseudo−first−order kinetics equation adsorption rate constant (min$^{-1}$), $k_2$—pseudo−second−order kinetics equation adsorption rate constant (g·mg$^{-1}$·min$^{-1}$).

## 3. Results and Discussion

### *3.1. Investigation of the Properties of CMC−nZVI*

The naked nZVI particles, which were roughly 100 nanometers in size and primarily spherical in shape, are shown in Figure 1a. However, nZVI particles have a tendency to group together and create clump−like agglomerates because of van der Waals forces and magnetic interactions [26]. These results are consistent with previous studies [27]. CMC−nZVI exhibited uniform dispersion with a low tendency to aggregate (Figure 1b), which is attributed to the significant increase in surface repulsion of the material after CMC coating of nZVI, resulting from both electrostatic potential repulsive effects and steric potential repulsive effects [28]. It is also worth noting that nZVI and CMC−nZVI had specific surface areas of 11.48 and 51.58 $m^2 \cdot g^{-1}$, respectively. The result was related to the use of the CMC coating material, which effectively prevents nZVI agglomeration [29]. This aligns with the findings from the SEM study.

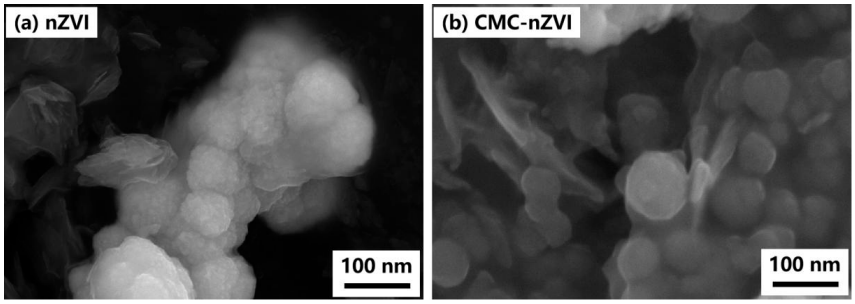


**Figure 1.** SEM images of (**a**) nZVI and (**b**) CMC−nZVI.

Figure 2 shows the XRD profiles of nZVI and CMC−nZVI. nZVI and its CMC−modified counterpart both displayed diffraction patterns associated with the BCC lattice of the α−Fe phase, specifically the (110) crystallographic plane, which is indicative of iron in its zero−valent state being the predominant constituent, characterized by distinctive peaks within the 2θ range of 45 °~46°. The peak of $Fe_2O_3$ appeared in the nZVI spectrum, indicating that some of the nZVI has been oxidized during the sample preparation. The effective inclusion of the carbon−containing polymeric substance CMC was demonstrated by the development of the C peak in the CMC−nZVI spectrum. Furthermore, the $Fe^0$ peak in the CMC−nZVI spectrum was not distinct, which was due to the incorporation of organic matter.

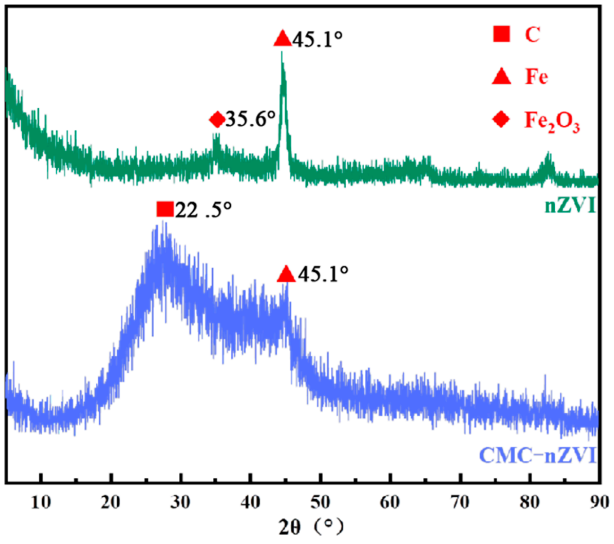


**Figure 2.** XRD profiles of nZVI and CMC−nZVI.

Figure 3 illustrates the XPS patterns of nZVI and CMC−nZVI. Both materials have five forms of iron: FeOOH, Fe(III), Fe(II), $Fe_2O_3$, and $Fe^0$. The total percentage of $Fe^{2+}$ and $Fe^0$ in CMC−nZVI was 32.29%, and the total percentage of $Fe^{2+}$ and $Fe^0$ in nZVI was only 9.10%, which was 23.19% higher than bare nZVI. The $Fe^0$ content rose from 0.07% to 12.63%, suggesting that the CMC coating decreased the oxidation of nZVI.

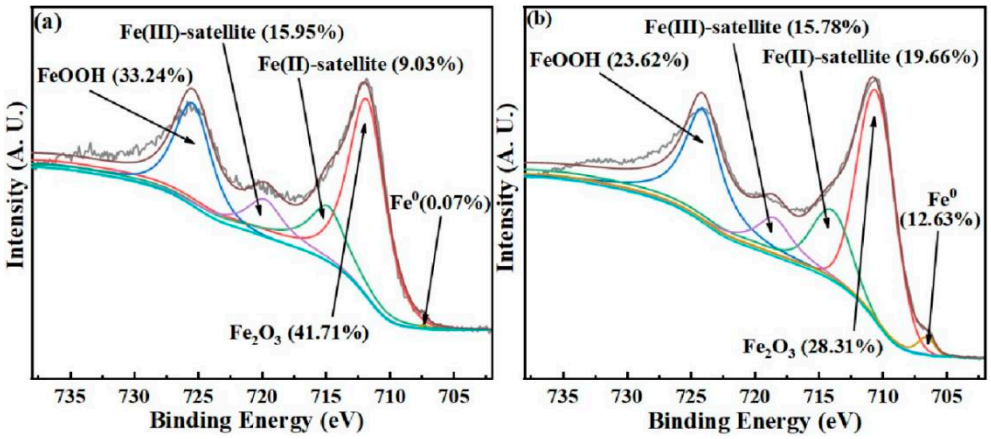


**Figure 3.** XPS pattern of (**a**) nZVI and (**b**) CMC−nZVI.

Figure 4 illustrates the anodic polarization curves of nZVI and CMC−nZVI. In the electrochemical analyzer, the oxidation reaction occurred at the anode. This reflects the stability of CMC−nZVI and bare ZVI at a specific voltage. Figure 4b suggests that the oxidation potential of CMC−nZVI (1.70 V) was higher than bare nZVI (1.55 V), indicating that CMC−nZVI was present in the soil for a longer time and had a longer effective action time.

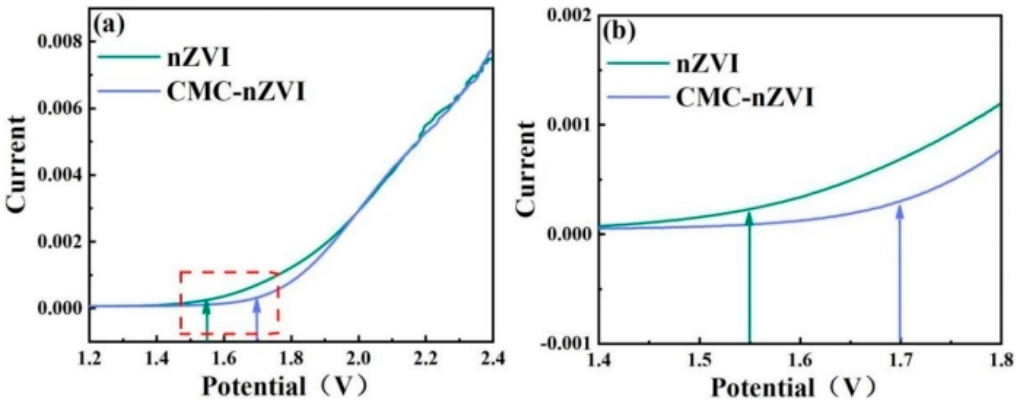


**Figure 4.** LSV anodic polarization curves of nZVI and CMC−nZVI. (**b**) An enlarged view of the dashed box in (**a**).

### *3.2. Coating Ratio Investigation Results*

Figure 5 shows the antioxidant properties of bare nZVI (control sample) and CMC−nZVI (mass ratio $M_{CMC}$:$M_{iron}$ = 0.5:1, 1:1, and 2:1). The four experimental groups in this study were in the same environment and were exposed to air. Other factors were controlled identically during the experiments, such as specimen mass, vessel type, placement, etc. The color of bare nZVI changed from black to brown after 1 h, as it had been oxidized completely. The oxidation duration of nZVI was prolonged by the addition of CMC. Additionally, nZVI's antioxidant qualities gradually improved as the dosage of CMC was raised. It was observed that when the mass ratio of CMC to nZVI was in excess of 2:1, the CMC−nZVI storage time in the air was found to be longer than 5 days.

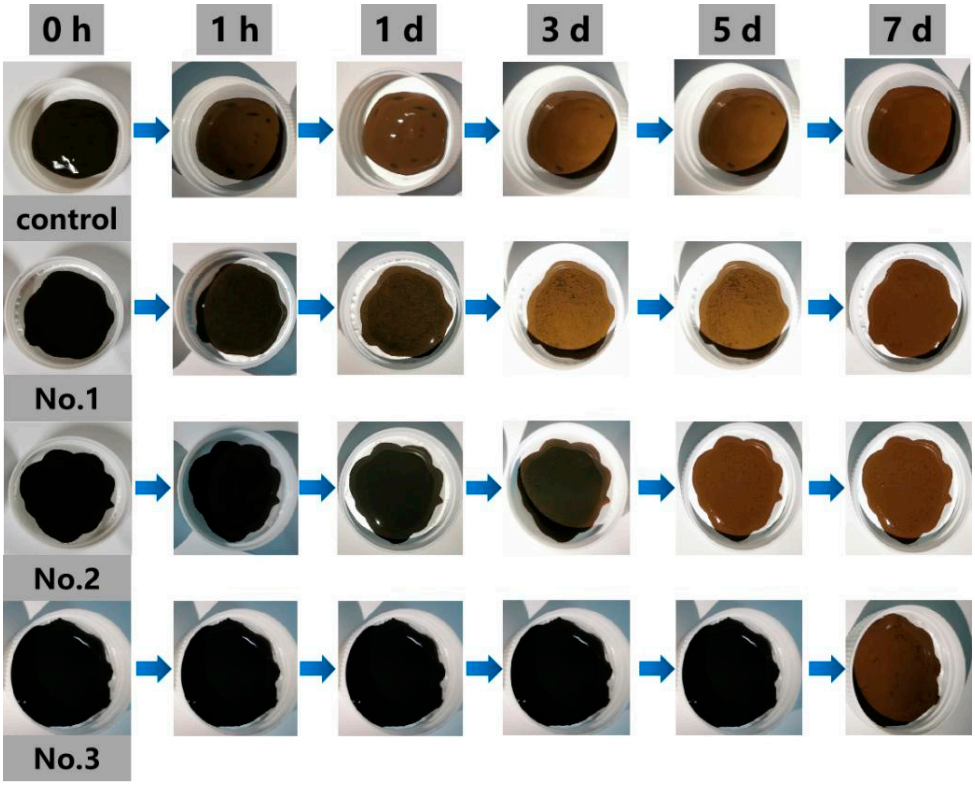


**Figure 5.** Images of antioxidant properties of different materials.

Figure S1 displays the outcomes of CMC and nZVI's elimination of Cr(VI) from the solution at various ratios. The adsorption capacity and removal rate of Cr(VI) increased as the mass ratio of CMC to nZVI was raised, as shown in Figure S1a–c. This implies that CMC enhances the CMC−nZVI adsorption performance and prevents nZVI from clumping together. The clearance rate of Cr(VI) reached 98.5% in 90 min when the mass ratio of CMC to nZVI was 1:1. Increasing the mass ratio to 2:1 had little further effect on the Cr(VI) removal efficiency. Simultaneously, 101.12 $mg \cdot g^{-1}$ was the new adsorption capacity, up from 100.88 $mg \cdot g^{-1}$. The results indicated that the viscosity of CMC−nZVI increased after the cladding ratio exceeded 1:1, which affected the fluidity and dispersion of the material in the solution and did not significantly enhance the removal effect. As a result, 1:1 was the ideal ratio for carrying out further trials.

### *3.3. Experiments for Cr(VI) Removal in Soils Investigation Results*

At CMC−nZVI doses of 0.5, 1.0, 1.5, and 3.0 $g \cdot kg^{-1}$, the equilibrium adsorption capacities and removal efficiencies of Cr(VI) are shown in Figure S2a–c. The rate at which Cr(VI) is removed was found to rise as the dosage of CMC−nZVI increased. After 10 h, 66.6% of Cr(VI) was eliminated with a CMC−nZVI dosage of 1.5 $g \cdot kg^{-1}$, but only 43.2% was eliminated with a dosage of 0.5 $g \cdot kg^{-1}$. The rationale is that as the CMC−nZVI dosage increases, the number of active sites increases, which greatly improves the removal rate of Cr(VI) [30]. However, the elimination (%) by 8 h was little impacted by additional CMC−nZVI dosage increases (over 1.5 $g \cdot kg^{-1}$). As the dose increased, CMC−nZVI's adsorption ability for Cr(VI) dropped from 146.6 to 39.17 $mg \cdot g^{-1}$ (Figure S2c). This reason for this is a reduction in the quantity of Cr(VI) adsorbed per unit mass of CMC−nZVI. In light of the cost of CMC−nZVI and the Cr(VI) removal efficiency, it seems reasonable to suggest that a dosage of 1.5 $g \cdot kg^{-1}$ may be an appropriate option.

Figure S2d–f shows the elimination rates and the sorption capacity at equilibrium of CMC−nZVI for various levels of Cr(VI). The maximum efficiencies for decolorization reached after 10 h were 73.2%, 66.6%, 59.3%, and 39.8% at initial concentrations of 101.2, 169.5, 202.2, and 315.2 $mg \cdot L^{-1}$, respectively. It appears that the high initial concentration

of Cr(VI) may have contributed to the saturation of adsorption sites on the CMC−nZVI surface. Each concentration of CMC−nZVI had an adsorption capacity of 49.4 $mg \cdot g^{-1}$, 75.3 $mg \cdot g^{-1}$, and 80.0 $mg \cdot g^{-1}$. One possible explanation for this phenomenon is that the higher starting Cr(VI) concentration may have contributed to an increased mass transfer barrier for the Cr(VI) molecules to overcome when approaching the CMC−nZVI surface [18]. As a result, the adsorptive capacity of CMC−nZVI increased in relation to the initial concentration of Cr(VI).

Figure S2g–i shows how CMC−nZVI affects the equilibrium adsorption capacity and removal rate of Cr(VI) at various soil pH levels. The adsorption capacity dropped from 105.3 to 48.5 $mg \cdot g^{-1}$ and the Cr(VI) removal rate dropped from 93.2% to 42.9% when the pH rose from 3.3 to 10.1. The pH value significantly impacts the redox interaction between nZVI and Cr(VI), which is similar to the conclusions of other customized nZVI in removing Cr(VI) [31,32]. On the one hand, in an acidic environment, a high $H^+$ concentration in the soil might hasten the disintegration of the inert oxide covering on the nZVI surface. $Fe^0$ exposure promotes electron release, which makes it easier for nZVI and Cr(VI) to come into contact and improves removal efficiency. On the other hand, $H^+$ has the ability to neutralize $OH^-$ and lessen the production of hydroxide precipitates. Alkaline circumstances promoted the hydroxide precipitates $Fe(OH)_3$ and $Cr(OH)_3$, which could potentially coat the surface of nZVI, prevent the transport of electrons from $Fe^0$ to Cr(VI), and render nZVI inactive.

### *3.4. Adsorption Kinetics Analysis*

The process of elimination of Cr(VI) progressed rapidly for the initial two hours and approached the removal equilibrium after four hours, as shown in Figure S2a,d,g. This is because there were a lot of adsorption and reduction sites on CMC−nZVI during the first removal stage. Furthermore, the high concentration of CMC−nZVI in the soil increased the mass transfer driving force between the Cr(VI) and the interfacial material, facilitating the extraction of heavy metal ions [33]. During the elimination process, the oxidation of the $Fe^0$ on the surface of CMC−nZVI caused the reactive sites to finally become saturated. Consequently, the efficacy of eradicating Cr(VI) was restricted.

Given the significant effect that pH has on the removal of Cr(VI) by CMC−nZVI, an adsorption kinetics analysis was conducted with pH as a variable. Appropriate parameters were obtained from the pseudo−first (4) and pseudo−second (5) order kinetic models. The results of the kinetic model fitting are depicted in Figure 6, while the parameters derived from kinetics at varying initial pH values are detailed in Table S2. Comparing the data of the pseudo−first and the pseudo−second−order kinetic model, the latter had a correlation coefficient between 0.997 and 0.998. Since the actual value of $Q_e$ was comparable to the theoretical value, and the kinetic model matched the pseudo−second−order kinetics well, the removal of Cr(VI) from soil by CMC−nZVI was a chemisorption process that included both chemical reduction and physical adsorption. This process is determined by two factors: one is determined by electron transfer and valence bonding forces, and the other is determined by physical diffusion [34]. Figure 7 illustrates the fitting results of the adsorption isotherm curve model. The parameters obtained from the isothermal adsorption model under different initial concentrations are shown in detail in Table S3. In contrast to the Freundlich isothermal adsorption model, the Langmuir isothermal adsorption model had an $R^2$ greater than 0.95. Compared to the Freundlich model, it is more accurate in describing the adsorption process. At 123.465 $mg \cdot g^{-1}$, the $q_m$ value was more in line with the experimental value. This suggests that the monolayer homogeneous chemical adsorption occurred at locations on the CMC−nZVI surface and that no communication occurred between the adsorbate molecules. Combined with Table S2, it can be known that removing Cr(VI) from the soil by CMC−nZVI is a chemical adsorption process. In comparison to other materials, CMC−nZVI has been observed to have a greater adsorption capacity for Cr(VI) removal. This can be attributed to the distinctive nature of the nZVI material and the CMC loading of nZVI.

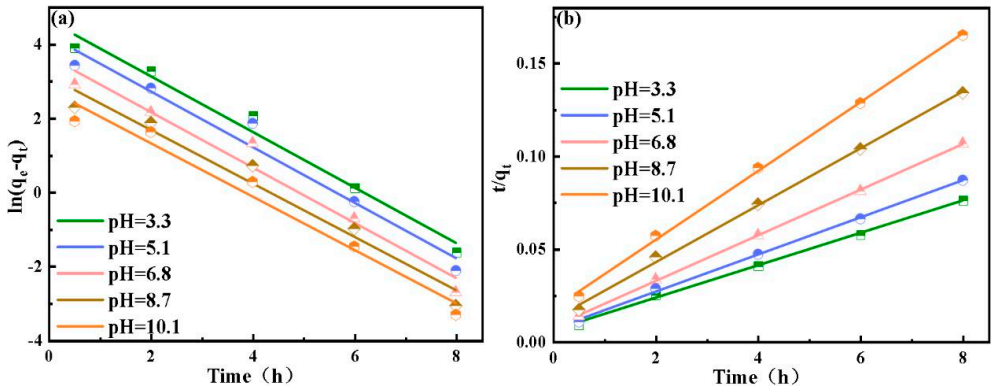


**Figure 6.** (**a**) Pseudo−first−order kinetics model and (**b**) pseudo−second−order kinetics model.

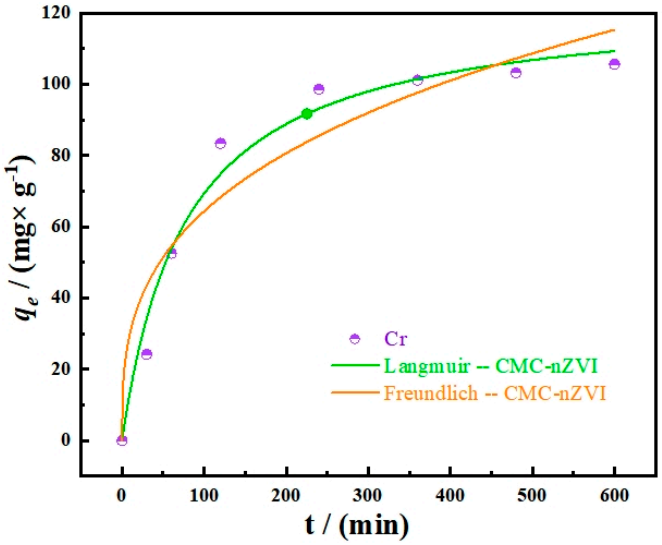


**Figure 7.** The adsorption isotherm of Cr (pH = 3.3, T = 25 °C) conforms to the Langmuir and Freundlich models.

## 4. Mechanism Analysis

Further investigation was conducted into the Cr(VI) removal process using CMC−nZVI, SEM−EDS, XRD, and XPS spectroscopy. The materials used for the aforementioned characterization were separated using a magnet. Please refer to Figure 8 for the SEM−EDS spectra of CMC−nZVI before and after the reaction with Cr(VI). Prior to the reaction, there was no aggregation of nZVI particles, and the particle size was decreased because of the dispersive impact of CMC (Figure 8a). Following the reaction of Cr(VI), the morphology of the material changed, and a large amount of fluffy material was produced, which was caused by the oxidation of $Fe^0$ by $Cr^{6+}$ and was also considered to be the complex hydroxide precipitates of Fe−Cr, further proving that the removal process contained a redox reaction (Figure 8b). Comparing spectra 1 and 2 in Figure 8c, spectra 2 show a noticeable decrease in the Fe peak and an increase in the Cr peak. In addition to the Fe, O, and C components, the CMC−nZVI−Cr surface also contained a notable amount of Cr elements, which were distributed quite evenly (Figure 8d). The elimination mechanism was shown to involve adsorption as a result of CMC−nZVI's reaction with Cr(VI) and showed adsorption of Fe−Cr complexes on the surface.

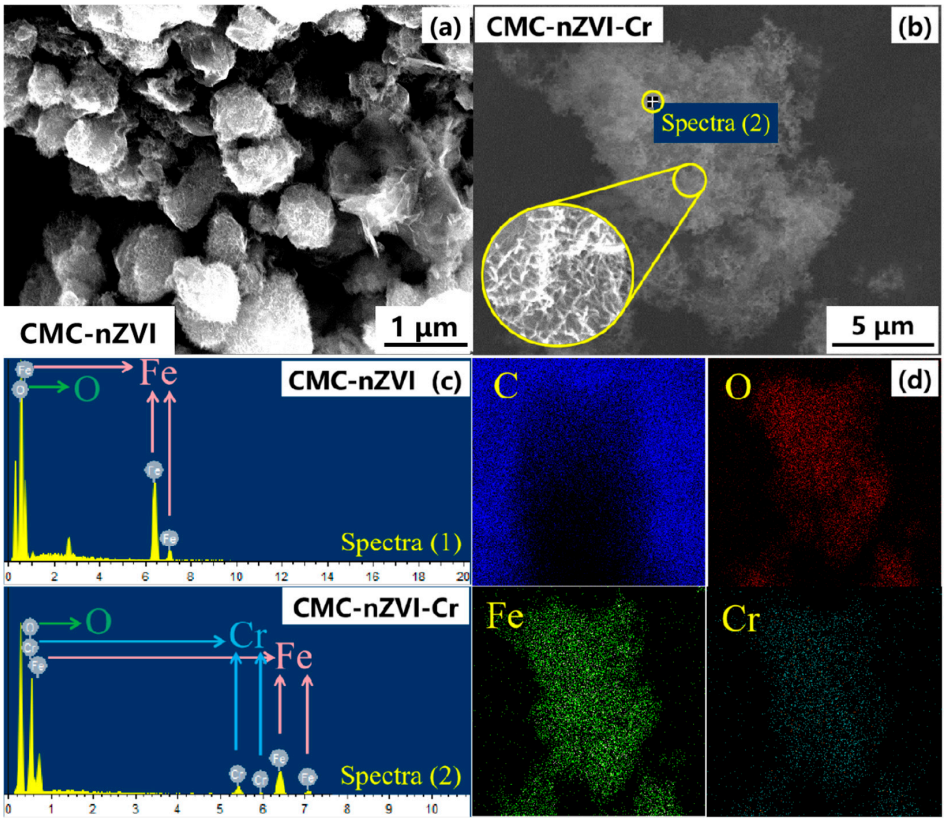


**Figure 8.** (**a**) SEM images of CMC−nZVI and (**b**) CMC−nZVI−Cr and (**c**,**d**) EDS images of CMC−nZVI−Cr. In (**d**), the blue color represents the C element, the red color represents the O element, the green color represents the Fe element, and the cyan color represents the Cr element.

Figure 9 displays the CMC−nZVI and CMC−nZVI−Cr XRD patterns. The peak of $Fe^0$ vanished when CMC−nZVI interacted with Cr(VI). The peak associated with $Fe_2O_3$ increased at 2θ = 43.1°, where Fe was present as a positive trivalent. This indicates that a redox process with Cr(VI) within the soil caused $Fe^0$ to be consumed. Fe(III) was produced by oxidizing $Fe^0$.

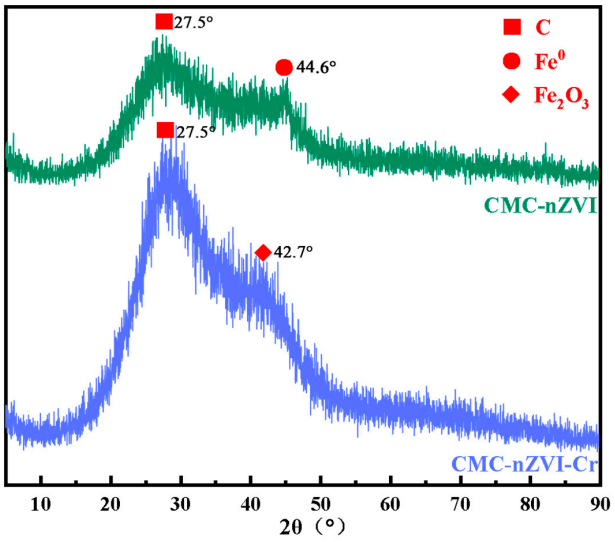


**Figure 9.** XRD images of CMC−nZVI and CMC−nZVI−Cr.

Figure S3 exhibits the XPS analysis, which was performed before and after interacting with Cr(VI) and CMC−nZVI. Figure S3a,b illustrate the overall spectra of CMC−nZVI and CMC−nZVI−Cr, respectively. The comparison revealed that the appearance of a Cr peak (b) confirmed that CMC−nZVI adsorbs Cr, which supports the aforementioned XRD analysis. In the iron spectrum shown in Figure S3c, it can be observed that there are five peaks present, namely $Fe^0$ at 707 eV (12.63%), $Fe_2O_3$ at 711 eV (28.31%), Fe(II)−satellite at 714 eV (19.66%), Fe(III)−satellite at 718 eV (15.78%), and FeOOH at 724 eV (23.62%). When the Cr(VI) was removed (Figure S3d), the $Fe^0$ peak at 707 eV disappeared, the Fe(II) content decreased, and the $Fe_2O_3$ content increased. This implies that over the course of treatment, Cr(VI) oxidized $Fe^0$ and Fe(II). After the reaction of Cr(VI) with CMC−nZVI (Figure S3e), the binding energy peaked at 576 eV for Cr(III) ($Cr_xFe_{1-x}(OH)_3$ and $FeCr_2O_4$) and 586 eV for Cr(VI) based on the percentage of Cr in different valence states. The fact that 70.72% of Cr(III) was adsorbed on the material's surface further demonstrates that a sizable portion of Cr(VI) was decreased.

Both the kinds of metal ions that are present in the soil and the effectiveness of CMC−nZVI are significantly impacted by pH. This also has a significant impact on the removal of metal ions. The Cr−$O_2$−$H_2O$ system's E−pH diagram is shown in Figure 10. $HCrO_4^-$ and $CrO_4^{2-}$ are the predominant forms of Cr(VI) in the pH ranges of 2~6.47 and 6.47~14. Under acidic conditions, $Fe^0$ is more easily oxidized to Fe(II) or Fe(III), releasing electrons. Chromate anions, such as $HCrO^{4-}$, $CrO4^{2-}$, and others, acquire electrons in the soil, converting Cr(VI) to Cr(III) (Equations (6)–(9)). But in alkaline circumstances, a lot of $OH^-$ causes hydroxide precipitates of Fe(II), Fe(III), and Cr(III) to form (Equations (10)–(12)). These precipitates cover the surface of nZVI to stop electron transfer and lower its activity. Meanwhile, the complex precipitation of Fe(III) and Cr(III) forms (Equations (13) and (14)). These complexes are extremely stable and are not easily re−dissolved into the ionic state so that the heavy chromium metal can be effectively removed. Since the materials used for characterization are involved in the reaction under weakly alkaline conditions, a hydroxide complex of iron−chromium is present in the characterization results.

$$2HCrO_4^- + 3Fe^0 + 14H^+ \rightarrow 3Fe^{2+} + 2Cr^{3+} + 8H_2O \quad (6)$$

$$HCrO_4^- + 3Fe^{2+} + 7H^+ \rightarrow 3Fe^{3+} + Cr^{3+} + 4H_2O \quad (7)$$

$$2CrO_4^{2-} + 3Fe^0 + 8H_2O \rightarrow 3Fe^{2+} + 2Cr^{3+} + 16OH^- \quad (8)$$

$$CrO_4^{2-} + 3Fe^{2+} + 4H_2O \rightarrow 3Fe^{3+} + Cr^{3+} + 8OH^- \quad (9)$$

$$Fe^{2+} + 2OH^- \rightarrow Fe(OH)_2 \downarrow \quad (10)$$

$$Fe^{3+} + 3OH^- \rightarrow Fe(OH)_3 \downarrow \quad (11)$$

$$Cr^{3+} + 3OH^- \rightarrow Cr(OH)_3 \downarrow \quad (12)$$

$$(1-x)Fe^{3+}{}_{(ag)} + xCr^{3+}{}_{(ag)} + 3H_2O \rightarrow Cr_xFe_{1-x}(OH)_3 \downarrow + 3H^+{}_{(ag)} \quad (13)$$

$$(1-x)Fe^{3+}{}_{(ag)} + xCr^{3+}{}_{(ag)} + 2H_2O \rightarrow Cr_xFe_{1-x}(OOH) \downarrow + 3H^+{}_{(ag)} \quad (14)$$

The mechanism by which CMC−nZVI removes Cr(VI) from soil encompasses three primary effects, as illustrated in Figure 11. (1) Redox effect: nZVI has a strong reducing property and reduces the highly mobile Cr(VI) in the soil to the stable Cr(III) by releasing electrons. (2) Adsorption: the large specific surface area and tiny particle size of CMC−nZVI provide it with a powerful adsorption capability. This capability is particularly evident at the onset of the reaction, where the surface of nZVI adsorbs a significant amount of Cr(VI) to facilitate electron transfer. (3) Complexation precipitation effect: a portion of Fe(III) and Cr(III) forms hydroxide precipitates ($Fe(OH)_3$ and $Cr(OH)_3$) that adhere to the soil. Another portion, due to the presence of $OH^-$ ions in the soil, forms iron−chromium hydroxide complexes ($Cr_xFe_{1-x}(OH)_3$). These complexes are relatively stable and less likely to be re−leached into the ionic state, thereby achieving the goal of immobilizing chromium.

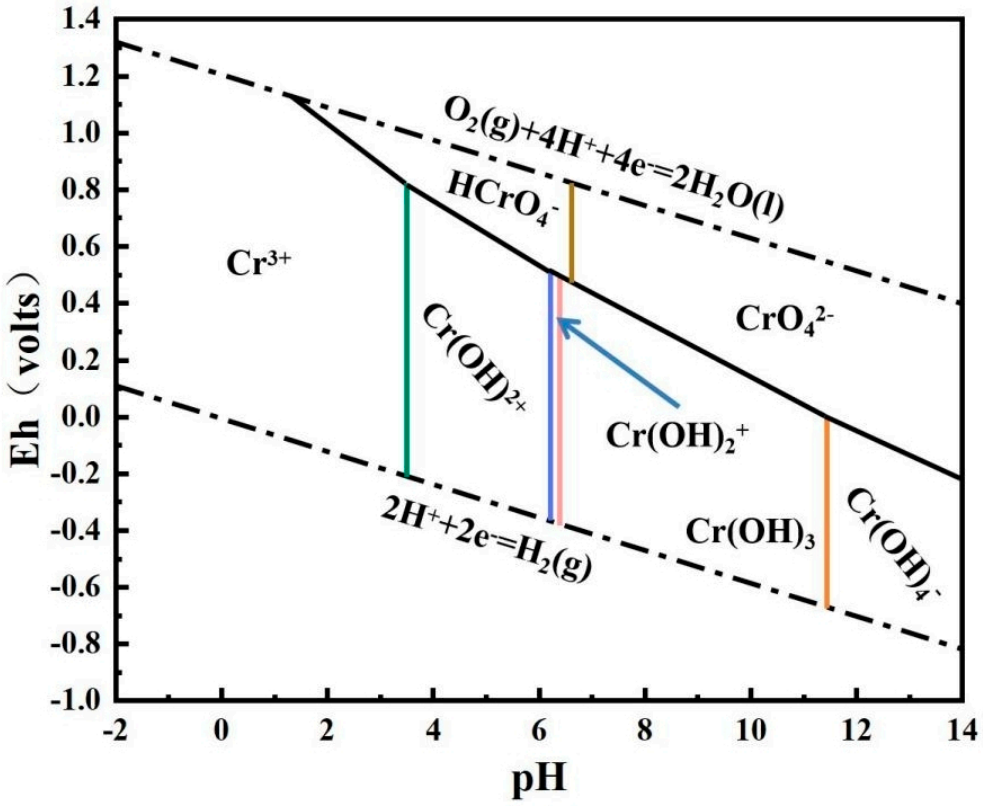


**Figure 10.** E−pH diagram of the Cr−$O_2$−$H_2O$ system.

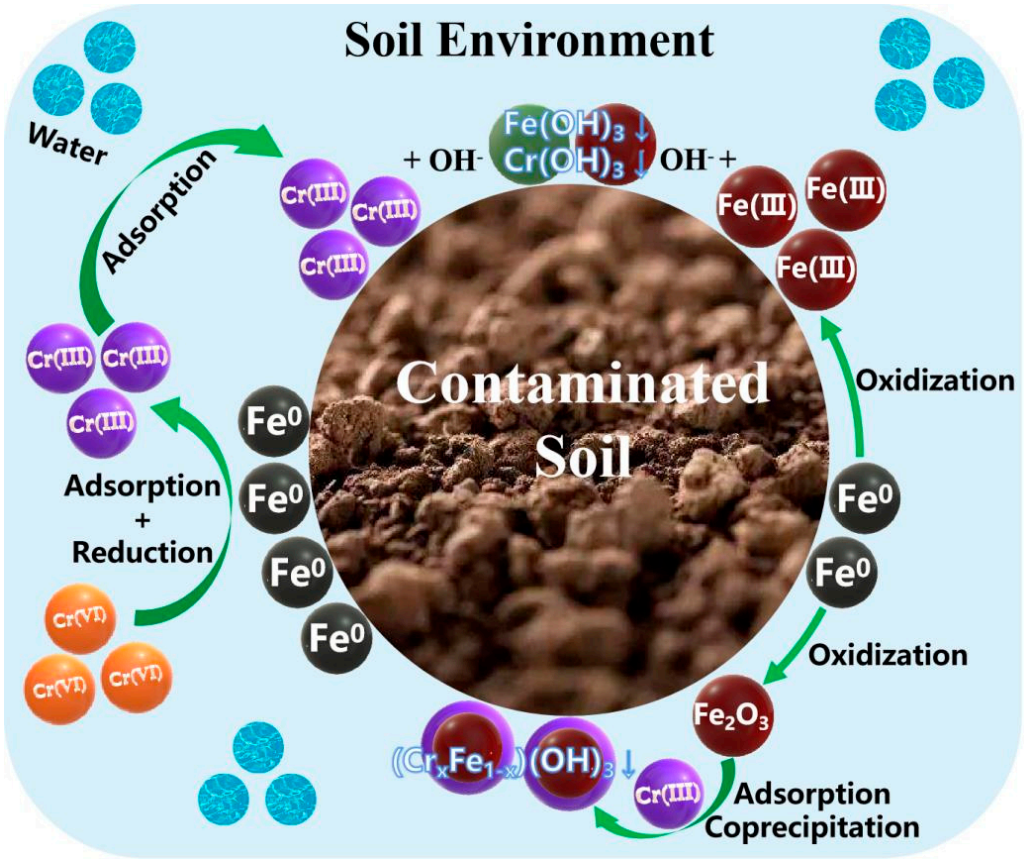


**Figure 11.** Removal mechanism for Cr(VI) by CMC−nZVI in soil.

## 5. Conclusions

CMC−nZVI was effectively synthesized in this work, and its effectiveness in eliminating Cr(VI) under several circumstances was examined. CMC may improve antioxidant capacity, stop nZVI from aggregating, and increase the likelihood that contaminants will interact with nZVI. As the CMC−nZVI dosage and reaction time rose, the removal efficacy of Cr(VI) improved proportionately, even if the pH value and concentration of Cr(VI) dropped. Additionally, the CMC−nZVI elimination process of Cr(VI) was more in line with the pseudo−second−order kinetic model than it was with them. Compared to the Freundlich mode, the experimental results in this investigation were more consistent with the Langmuir isothermal adsorption model. This suggests that the removal of hexavalent chromium is governed by a chemisorption mechanism. Two factors determine this process: one is determined by electron transfer and valence bonding forces and the other by physical diffusion. Furthermore, because an alkaline environment promotes complexation precipitation and an acidic environment promotes electron transfer (redox), pH is crucial in the removal of Cr(VI). Further research on the mechanism of CMC−nZVI for removing hexavalent chromium from soil indicates that the removal process involves three mechanisms: redox, adsorption, and complexation precipitation. In summary, CMC−nZVI has great application prospects in effectively removing hexavalent chromium from soil.

**Supplementary Materials:** The following supporting information can be downloaded at: https://www.mdpi.com/article/10.3390/cleantechnol6040078/s1, Table S1: Information about the chemicals used in the experiment; Table S2: Fitting results of the kinetic equation under different pH; Table S3: Isotherms parameters for Cr adsorption onto CMC−nZVI; Figure S1: (a) Comparison of Cr(VI) removal using CMC-nZVI with various ratios (CMC:nZVI mass ratio). With a pH of 7, an initial Cr(VI) content of 128 mg·$L^{-1}$, and a temperature of 20 °C, the dosage of nZVI and CMC-nZVI is 1.25g·$L^{-1}$; (b) Removal rate of different coated ratio; (c) Equilibrium adsorption of different coated ratio; Figure S2: Effect of Different Factors on CMC−nZVI's Cr(VI) Removal; Figure S3: XPS Spectra of CMC−nZVI Before and After Cr(VI) Reaction.

**Author Contributions:** Writing—review & editing, Funding acquisition and Supervision, B.Z. (Bo Zhang); Writing—review & editing, Validation, Visualization and Conceptualization, J.Z.; Writing—original draft, Validation, Methodology and Conceptualization, J.F.; Formal analysis, Project administration and Supervision, B.Z. (Bohong Zhu); Conceptualization, Formal analysis and Investigation, W.S.; Validation, Conceptualization and Investigation, S.Z. and W.L.; Project administration and Supervision, Z.L. and F.Z. All authors have read and agreed to the published version of the manuscript.

**Funding:** This work was supported by the Provincial Special Project of Chenzhou National Sustainable Development Agenda Innovation Demonstration Zone Construction (NO. 2022sfq44), the Hunan Natural Science Foundation of China (No. 2022JJ40143), and the Project of Hunan Provincial Department of Education (No. 23B0539).

**Data Availability Statement:** This article contains all of the data generated or analyzed during this study.

**Conflicts of Interest:** Author Zhaohui Li and Fanjun Zeng are employed by the company Linwu Xiangxin Kaishun Water Service Co. The authors declare no conflicts of interest, namely, no personal or collaborative conflicts, no professional or commercial conflicts, or any other conflicts of interest.

## References

1. Lyu, H.; Zhao, H.; Tang, J.; Gong, Y.; Huang, Y.; Wu, Q.; Gao, B. Immobilization of hexavalent chromium in contaminated soils using biochar supported nanoscale iron sulfide composite. *Chemosphere* **2018**, *194*, 360–369. [CrossRef] [PubMed]
2. Hepburn, E.; Northway, A.; Bekele, D.; Liu, G.-J.; Currell, M.J. A method for separation of heavy metal sources in urban groundwater using multiple lines of evidence. *Environ. Pollut.* **2018**, *241*, 787–799. [CrossRef] [PubMed]
3. Ahmadi, S.; Jahanshahi, R.; Moeini, V.; Mali, S. Assessment of hydrochemistry and heavy metals pollution in the groundwater of Ardestan mineral exploration area, Iran. *Environ. Earth Sci.* **2018**, *77*, 1–13. [CrossRef]
4. Wang, F.; Yang, W.; Zheng, F.; Sun, Y. Removal of Cr (VI) from Simulated and Leachate Wastewaters by Bentonite-Supported Zero-Valent Iron Nanoparticles. *Int. J. Environ. Res. Public Health* **2018**, *15*, 2162. [CrossRef]
5. Kumar, A.; Gahoi, P.; Verma, N. Simultaneous scavenging of Cr(VI) from soil and facilitation of nutrient uptake in plant using a mixture of carbon microfibers and nanofibers. *Chemosphere* **2019**, *239*, 124760. [CrossRef]

6. Wang, S.; Zhao, M.; Zhou, M.; Li, Y.C.; Wang, J.; Gao, B.; Sato, S.; Feng, K.; Yin, W.; Igalavithana, A.D.; et al. Biochar-supported nZVI (nZVI/BC) for contaminant removal from soil and water: A critical review. *J. Hazard. Mater.* **2019**, *373*, 820–834. [CrossRef]
7. Zhang, S.; Lyu, H.; Tang, J.; Song, B.; Zhen, M.; Liu, X. A novel biochar supported CMC stabilized nano zero-valent iron composite for hexavalent chromium removal from water. *Chemosphere* **2019**, *217*, 686–694. [CrossRef]
8. Han, Y.; Zhou, X.; Lei, L.; Sun, H.; Niu, Z.; Zhou, Z.; Xu, Z.; Hou, H. Efficient activation of persulfate by calcium sulfate whisker supported nanoscale zero-valent iron for methyl orange removal. *RSC Adv.* **2020**, *11*, 452–461. [CrossRef]
9. Tunç, M.S.; Tepe, O. Removal of phenol from aqueous solution using persulfate activated with nanoscale zero-valent iron. *Desalination Water Treat.* **2017**, *74*, 269–279. [CrossRef]
10. Tarekegn, M.M.; Hiruy, A.M.; Dekebo, A.H. Nano zero valent iron (nZVI) particles for the removal of heavy metals (Cd2+, Cu2+ and $Pb^{2+}$) from aqueous solutions. *RSC Adv.* **2021**, *11*, 18539–18551. [CrossRef]
11. Liang, L.; Li, X.; Guo, Y.; Lin, Z.; Su, X.; Liu, B. The removal of heavy metal cations by sulfidated nanoscale zero-valent iron (S-nZVI): The reaction mechanisms and the role of sulfur. *J. Hazard. Mater.* **2020**, *404 Pt A*, 124057. [CrossRef]
12. Zhao, X.; Liu, W.; Cai, Z.; Han, B.; Qian, T.; Zhao, D. An overview of preparation and applications of stabilized zero-valent iron nanoparticles for soil and groundwater remediation. *Water Res.* **2016**, *100*, 245–266. [CrossRef] [PubMed]
13. Shang, J.; Zong, M.; Yu, Y.; Kong, X.; Du, Q.; Liao, Q. Removal of chromium (VI) from water using nanoscale zerovalent iron particles supported on herb-residue biochar. *J. Environ. Manag.* **2017**, *197*, 331–337. [CrossRef] [PubMed]
14. Liu, F.; Yang, J.-H.; Zuo, J.; Ma, D.; Gan, L.-L.; Xie, B.; Wang, P.; Yang, B. Graphene-supported nanoscale zero-valent iron: Removal of phosphorus from aqueous solution and mechanistic study. *J. Environ. Sci.* **2014**, *26*, 1751–1762. [CrossRef] [PubMed]
15. Bao, T.; Damtie, M.M.; Hosseinzadeh, A.; Wei, W.; Jin, J.; Vo, H.N.P.; Ye, J.S.; Liu, Y.; Wang, X.F.; Yu, Z.; et al. Bentonite-supported nano zero-valent iron composite as a green catalyst for bisphenol A degradation: Preparation, performance, and mechanism of action. *J. Environ. Manag.* **2020**, *260*, 110105. [CrossRef]
16. Zhang, M.; Yi, K.; Zhang, X.; Han, P.; Liu, W.; Tong, M. Modification of Zero Valent Iron Nanoparticles by Sodium Alginate and Bentonite: Enhanced Transport, Effective Hexavalent Chromium Removal and Reduced Bacterial Toxicity. *J. Hazard. Mater.* **2020**, *388*, 121822. [CrossRef]
17. Bian, H.; Wan, J.; Muhammad, T.; Wang, G.; Sang, L.K.; Jiang, L.; Wang, H.-Y.; Zhang, Y.; Peng, C.; Zhang, W.; et al. Computational study and optimization experiment of nZVI modified by anionic and cationic polymer for Cr(VI) stabilization in soil: Kinetics and response surface methodology (RSM). *Environ. Pollut.* **2021**, *276*, 116745. [CrossRef]
18. Zeng, S.; Zhong, D.; Xu, Y.L.; Zhong, N. Application of porous styrene resin loaded carboxymethyl cellulose-stabilized nano-zero-valent iron for highly efficient hexavalent chromium removal. *New J. Chem.* **2022**, 1319–1328. [CrossRef]
19. Gong, L.; Shi, S.; Lv, N.; Xu, W.; Ye, Z.; Gao, B.; O'Carroll, D.M.; He, F. Sulfidation enhances stability and mobility of carboxymethyl cellulose stabilized nanoscale zero-valent iron in saturated porous media. *Sci. Total Environ.* **2020**, *718*, 137427. [CrossRef]
20. Di Palma, L.; Gueye, M.T.; Petrucci, E. Hexavalent chromium reduction in contaminated soil: A comparison between ferrous sulphate and nanoscale zero-valent iron. *J. Hazard. Mater.* **2015**, *281*, 70–76. [CrossRef]
21. Sparks, D.L. *Methods of Soil Analysis, Part 3: Chemical Methods*; John Wiley & Sons: Hoboken, NJ, USA, 2020.
22. Weaver, R.W. *Methods of Soil Analysis, Part 4: Physical Methods*; John Wiley & Sons: Hoboken, NJ, USA, 2020.
23. *GB/T 23739-2009*; Soil Quality-Analysis of Available Lead and Cadmium Contents in Soils-Atomic Absorption Spectrometry. Standards Press of China: Beijing, China, 2009.
24. *GB 7467-87*; Water Quality-Determination of Chromium(VI)-1,5 Diphenylcarbohydrazide Spectrophotometric Method. Standards Press of China: Beijing, China, 1987.
25. Xu, H.; Gao, M.; Hu, X.; Chen, Y.; Li, Y.; Xu, X.; Zhang, R.; Yang, X.; Tang, C.; Hu, X. A novel preparation of S-nZVI and its high efficient removal of Cr(VI) in aqueous solution. *J. Hazard. Mater.* **2021**, *416*, 125924. [CrossRef] [PubMed]
26. Fan, J.; Zhang, B.; Zhu, B.; Shen, W.; Chen, Y.; Zeng, F. New Insight into the Mechanism for the Removal of Methylene Blue by Hydrotalcite-Supported Nanoscale Zero-Valent Iron. *Water* **2023**, *15*, 183. [CrossRef]
27. Chen, W.; Wang, X.; Yuan, Z. Preparation of nanoscale zero-valent iron particles with different coatings for removal of Cr(VI) from water. *Int. J. Nanotechnol.* **2016**, *13*, 923. [CrossRef]
28. Jiao, C.; Tan, X.; Lin, A.; Yang, W. Preparation of Activated Carbon Supported Bead String Structure Nano Zero Valent Iron in a Polyethylene Glycol-Aqueous Solution and Its Efficient Treatment of Cr(VI) Wastewater. *Molecules* **2019**, *25*, 47. [CrossRef]
29. Wu, W.; Han, L.; Nie, X.; Gu, M.; Li, J.; Chen, M. Effects of multiple injections on the transport of CMC-nZVI in saturated sand columns. *Sci. Total Environ.* **2021**, *784*, 147160. [CrossRef]
30. Yi, Y.; Wang, X.; Ma, J.; Ning, P. An efficient Egeria najas-derived biochar supported nZVI composite for Cr(VI) removal: Characterization and mechanism investigation based on visual MINTEQ model. *Environ. Res.* **2020**, *189*, 109912. [CrossRef]
31. Dong, H.; Deng, J.; Xie, Y.; Zhang, C.; Jiang, Z.; Cheng, Y.; Hou, K.; Zeng, G. Stabilization of nanoscale zero-valent iron (nZVI) with modified biochar for Cr(VI) removal from aqueous solution. *J. Hazard. Mater.* **2017**, *332*, 79–86. [CrossRef]
32. Zhang, Y.; Jiao, X.; Liu, N.; Lv, J.; Yang, Y. Enhanced removal of aqueous Cr(VI) by a green synthesized nanoscale zero-valent iron supported on oak wood biochar. *Chemosphere* **2019**, *245*, 125542. [CrossRef]

33. Wang, J.; Zheng, S.; Shao, Y.; Liu, J.; Xu, Z.; Zhu, D. Amino-functionalized $Fe_3O_4$@$SiO_2$ core-shell magnetic nanomaterial as a novel adsorbent for aqueous heavy metals removal. *J. Colloid Interface Sci.* **2010**, *349*, 293–299. [CrossRef]
34. Vilardi, G.; Di Palma, L.; Verdone, N. A physical-based interpretation of mechanism and kinetics of Cr(VI) reduction in aqueous solution by zero-valent iron nanoparticles. *Chemosphere* **2019**, *220*, 590–599. [CrossRef]